LONGITUDINAL EMITTANCE MEASUREMENT AT THE ATS*

W. B. Cottingame, J. H. Cortez, W. W. Higgins, O. R. Sander, and D. P. Sandoval, AT-2, MS H818
Los Alamos National Laboratory, Los Alamos, NM 87545

Summary

With increasing brightness, beam diagnostic techniques requiring interception of the beam become impractical. For H⁻ particle beams, solutions for this problem based on the phenomenon of photodissociation are now being investigated at the Los Alamos National Laboratory accelerator test stand (ATS). A laser can be used to selectively neutralize portions of the beam that can be characterized after the charged particles have been swept away. We have used this technique for measuring longitudinal emittance at the output of the ATS radio-frequency quadrupole (RFQ).

Introduction

To avoid the problems associated with interceptive diagnostics techniques for particle beams of high brightness, the laser-induced neutralization diagnostic approach (LINDA) is being developed for the ATS. In this approach, a laser beam is used to selectively neutralize through the photodissociation process a segment of the H⁻ particle beam, and the H° particles are subsequently segregated from the H⁻ beam at a beam deflection element. The beam parameters at the point of neutralization are then simply reconstructed by using only the drift distance for the neutralized portion of the particle beam. In principle, this technique can be used to reconstruct the complete 6-D phase-space density distribution by altering the spatial and/or temporal structure of the photon field traversing the particle beam and using the appropriate detector geometry.

Experimental Setup

Initially we have used this technique to measure the longitudinal parameters at the exit of the 2-MeV ATS RFQ. Before obtaining a longitudinal emittance for the ATS RFQ, we used LINDA to measure the current density versus longitudinal phase and longitudinal energy distributions. These results have been previously reported.[1] Figure 1 indicates the experimental layout and beam configurations for our measurements. A single transverse slice of the microstructure is neutralized with a 1.06-μm Nd:YAG mode-locked laser capable of output energies of up to 10 mJ for a single 32-ps pulse. A telescope and cylindrical lens are used to expand the laser beam to 7 mm in the transverse dimension and to a focus of less than 30 μm in the longitudinal dimensional at the point of intersection with the ≈3-mm particle beam, 5.7 cm from the exit of the RFQ. The neutralization fraction for the portion of H⁻ beam illuminated by the laser is estimated to be 0.99 (well into saturation) for the 1- to 3-mJ pulse used. At this power level, 10% variations in laser power has negligible effect, and reflections below the 1% level can be ignored.

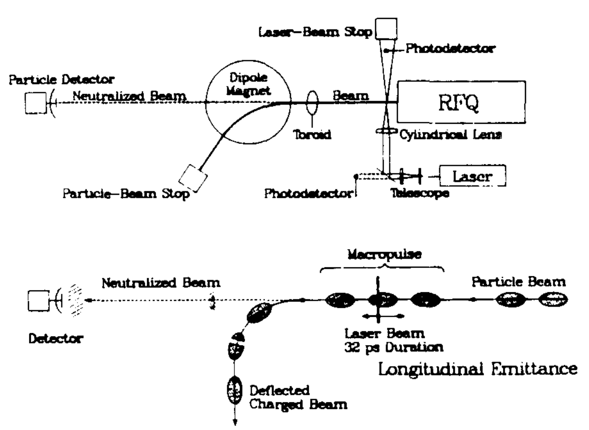

Fig. 1. Experimental layout and beam configuration for the longitudinal measurements.

The time at which the laser fires can be controlled only to within a few microseconds; therefore, the 413-MHz RFQ phase is random with respect to the time when the laser pulse traverses the particle beam. The relative phase for the sampled portion of the beam is determined by a computer-interfaced interval timer having approximately 15-ps resolution. (See logic diagram shown in Fig. 2.) An InP:Fe photodetector,

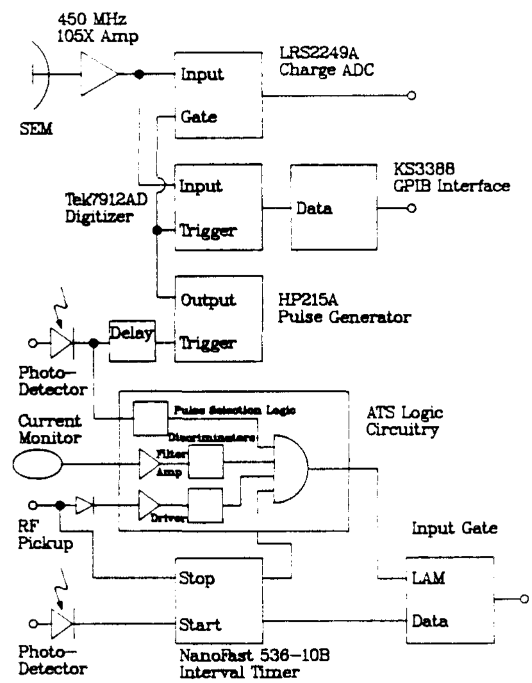

Fig. 2. Electronics diagram for longitudinal measurements.

having a rise time of less than 100 ps, is positioned in the laser beam downstream from the interaction point and is used to provide the start for the interval timer. The negative-going zero-crossing point of the vane potential as measured near the exit of the RFQ tank is used for the interval-timer stop point. System temporal resolution is estimated to be approximately 30 ps. To ensure laser, ion-source, and RFQ stability during data acquisition, additional electronic components are included to veto events for which the laser power, source current, or RFQ power fall below a predetermined discrimination level.

For longitudinal emittance measurements, the neutral-particle detection system consists of a subnanosecond secondary-emissions monitor (SEM) with an active area of 5.1 cm^2, a 450-MHz, 105X amplifier,

*Work performed under the auspices of the U.S. Dept. of Energy and supported by the U.S. Army Strategic Defense Command.

and a waveform digitizer interfaced to computer with IEEE Standard 488 interface (see Fig. 2). A second InP:Fe photodetector in the laser beam initiates data acquisition so that time-of-flight information can be taken from the digitized SEM waveform. A temporal dispersion in the 32-ps sample of the particle beam is produced by a 7.57-m drift between the point of neutralizátion and the SEM. Although this drift distance obviates the use of multigigahertz detection apparatus, less than 5% of the neutralized portion of the particle beam is collected.

Data Analysis

The relative phase and energy profiles are extracted from the interval timer values and the digitized waveforms in software. To build up an emittance profile, each waveform is binned in terms of phase and energy and averaged with any previous samples. The raw emittance plots (shown in Figs. 3 and 4) must be corrected to remove the 413-MHz rf background and the aberrations of the waveform digitizer. Additionally, secondary laser pulses (occurring at 7-ns intervals after the primary) produce artifacts in the data (the three additional peaks or islands that can be seen in Figs. 3 and 4) that must be removed. Because the tails of these distributions overlap at 1-5% of the peak values, the software cuts used to remove these artifacts are somewhat arbitrary at these levels.

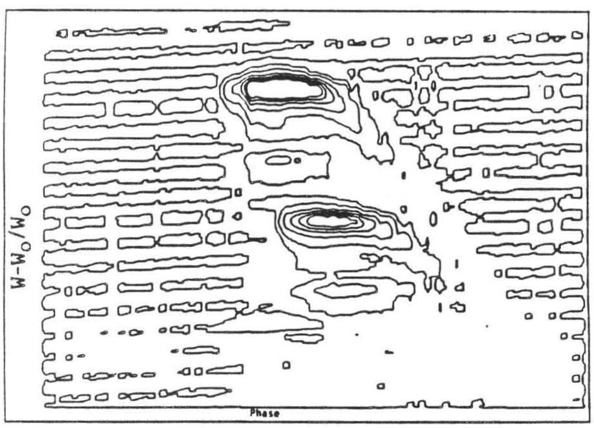

Fig. 3. Raw longitudinal emittance plot at 410-mV RFQ vane voltage.

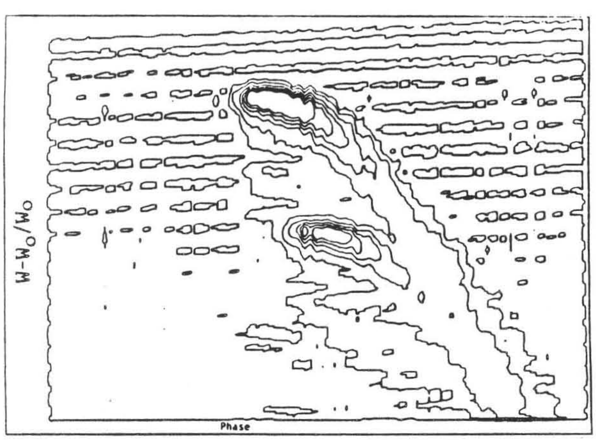

Fig. 4. Raw longitudinal emittance plot at 380-mV RFQ vane voltage.

Results

Figures 5 and 6 show isometric plots of the longitudinal emittance profile after background subtraction and software cuts have been implemented. Figure 5 is an emittance plot for an 82-mA, 2-MeV beam that was injected into the RFQ at 93.5 keV and was accelerated at an RFQ vane voltage assumed to be near the design value (410 mV at the power-sensitive rf pickup loop). Figure 6 is the result of a subsequent run with the same conditions except that the RFQ vane voltage was reduced (380 mV at the rf pickup loop) to a point above threshold for 2-MeV acceleration but

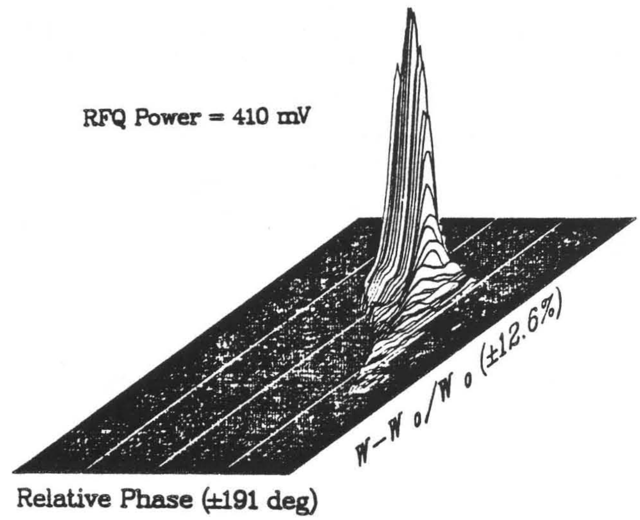

Fig. 5. Isometric longitudinal emittance plot at 410-mV RFQ vane voltage after background extraction and software cuts.

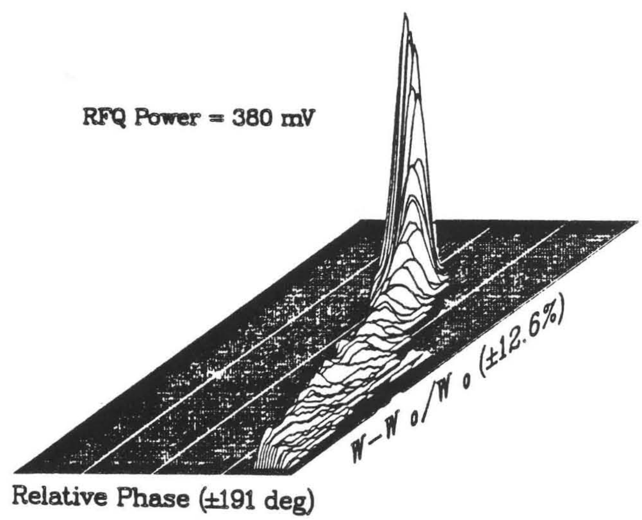

Fig. 6. Isometric Longitudinal emittance plot at 380-mV RFQ vane voltage after background extraction and software cuts.

below the design value. Table I gives the emittances, α's, β's, and beam contents for various contours for the 410-mV data. Units (for convenience of computation) are π•%(energy)•deg. In terms of π•MeV•deg, emittances and γ's should be divided by 50, and β's should be multiplied by 50. Figures 7 and 8 are contour plots of the same data. Figures 9 and 10 are projections onto the energy and phase axes.

TABLE I
LONGITUDINAL EMITTANCE PARAMETERS AT THE OUTPUT OF THE 2-MeV RFQ

THRESH	XAVE	XPAVE	BETA	GAMMA	ALPHA	ERMS	ETOT	THETA	C	SUMABOU	SUMTHRU
0.01	7.0634	5.794	26.1225	0.08	1.0819	39.1123	299.1614	87.625	26.17	34790.	34828.
MAXIMUM COUNTS	155.0000										
1.00	5.8085	5.856	24.8119	0.08	0.9862	35.1968	235.0641	87.720	24.85	31331.	34305.
2.00	3.4710	6.015	24.2286	0.07	0.7625	27.3806	169.7413	88.194	24.25	28238.	33031.
4.00	0.7061	6.209	24.9222	0.05	0.4712	19.1378	116.6742	88.915	24.93	25058.	30968.
6.00	0.6755	6.306	26.8953	0.04	0.3325	15.0137	90.0793	89.290	26.86	22427.	29263.
8.00	1.4827	6.372	28.6506	0.04	0.2758	12.8958	73.7792	89.440	28.65	20322.	27787
10.00	1.7171	6.415	30.5889	0.04	0.2765	11.5518	64.5875	89.482	30.59	18562.	26730.
12.00	2.0202	6.464	33.2734	0.03	0.2784	10.0440	55.0059	89.520	33.28	17044.	25526.
20.00	2.9863	6.536	34.8426	0.03	0.2061	7.3924	37.5024	89.661	34.84	12492.	21978.
30.00	-4.0021	6.594	37.0957	0.03	0.1298	5.4308	25.4918	89.799	37.10	8668.	18340.
40.00	-4.5579	6.633	40.6701	0.02	0.1021	4.2380	19.1189	89.856	40.67	5685.	15557
50.00	5.4062	6.663	43.9552	0.02	0.0475	3.2808	14.2166	89.938	43.96	3790.	12780.
60.00	6.1215	6.689	47.9442	0.02	0.0673	2.5122	10.5399	89.920	47.94	2212.	10210.
70.00	6.6138	6.694	51.8415	0.02	0.0358	1.8208	7.2309	89.960	51.84	1119.	7520.
80.00	5.0258	6.710	42.4031	0.02	0.0127	0.9428	3.5541	89.983	42.40	416.	4032.
90.00	6.8695	6.724	37.8861	0.03	0.0087	0.4110	1.7158	90.001	37.89	119.	2072

BEAM FRACTIONS 39.4%, 63.2%, 77.7%, 86.5%, 91.8%, 95.0%

THRESH	XAVE	XPAVE	BETA	GAMMA	ALPHA	ERMS	ETOT	THETA	C	SUMABOU	SUMTHRU
47.35	-4.8947	6.662	42.7782	0.02	0.1019	3.5488	15.4422	89.863	42.78	4281.	13528.
20.82	1.0781	6.540	35.0185	0.03	0.1988	7.0845	35.2964	89.674	35.02	12118.	21411
10.12	1.7171	6.415	30.5888	0.04	0.2765	11.5518	64.5875	89.482	30.59	18468.	26730.
5.52	-0.3881	6.285	26.4554	0.04	0.3573	15.8299	96.8199	89.225	26.46	23084.	29758.
3.49	1.3806	6.158	24.2640	0.05	0.5406	21.1211	128.9298	88.722	24.28	25875.	31568.
2.43	3.4710	6.015	24.2286	0.07	0.7625	27.3806	169.7413	88.194	24.25	27823.	33031

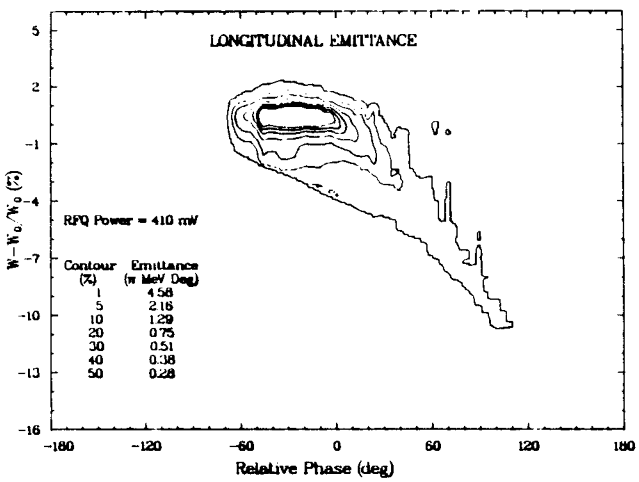

Fig. 7. Same as Fig. 5 except contour plot.

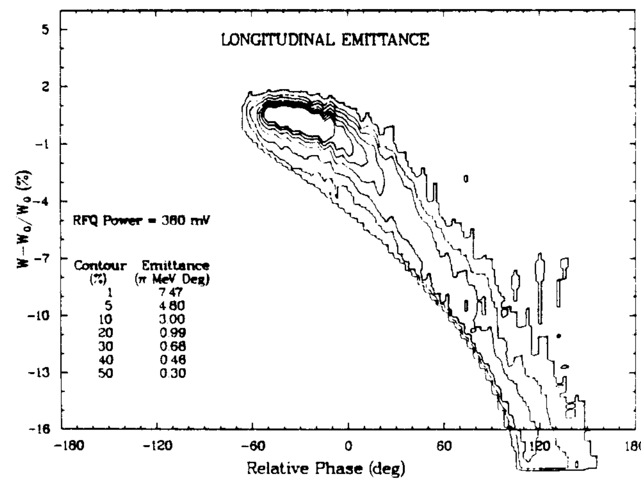

Fig. 8. Same as Fig. 6 except contour plot.

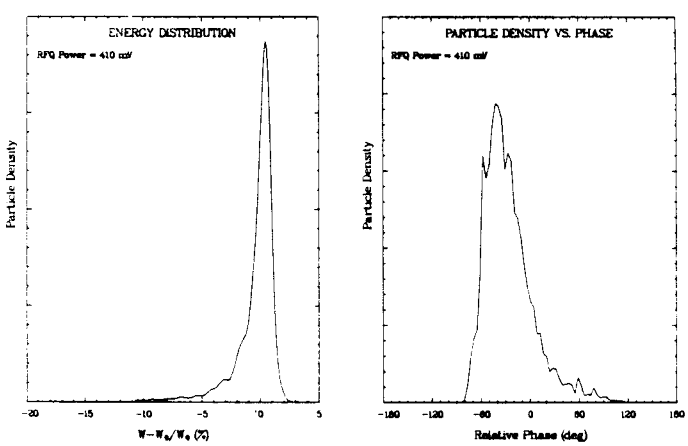

Fig. 9. Projection of 410-mV emittance data upon energy and phase axes.

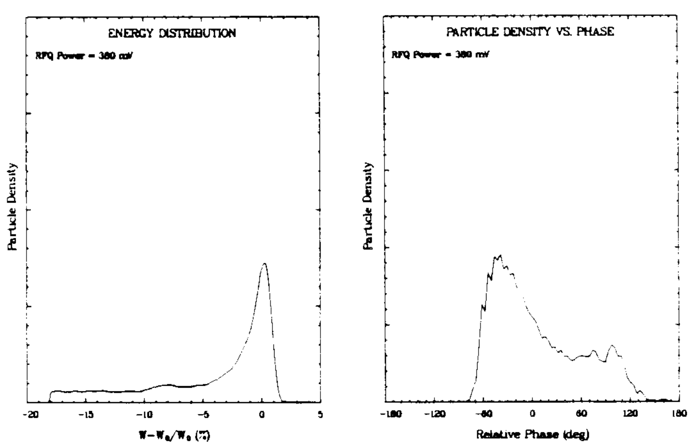

Fig. 10. Same as Fig. 9 except for 380-mV data.

Roughly, the results are as anticipated. The FWHM of the energy and phase distributions at the higher vane voltage are 1.25% and 50°, respectively. Below design vane voltage, the tails of both distributions increase as more particles fall from the bucket. Also, as expected, the γ's are small and the β's are large. However, to go beyond these statements will require both comprehensive calculations and more high-quality data.

REFERENCE

1. W. B. Cottingame, G. P. Boicourt, J. H. Cortez, W. W. Higgins, O. R. Sander, and D. P. Sandoval, "Noninterceptive Techniques for the Measurement of Longitudinal Parameters for Intense H^- Beams," Proc. 1985 Particle Accelerator Conference, IEEE Trans. Nucl. Sci. 32 (5), 1871 (1985).